

## Transparent superhydrophobic/superhydrophilic TiO<sub>2</sub>-based coatings for self-cleaning and anti-fogging†

Yuekun Lai,<sup>\*ab</sup> Yuxin Tang,<sup>a</sup> Jiaojiao Gong,<sup>c</sup> Dangguo Gong,<sup>a</sup> Lifeng Chi,<sup>b</sup> Changjian Lin<sup>c</sup> and Zhong Chen<sup>\*a</sup>

Received 1st December 2011, Accepted 7th February 2012

DOI: 10.1039/c2jm16298a

A stable titanate nanobelt (TNB) particle suspension was prepared by a hydrogen-bond-driven assembly of pre-hydrolysed fluoroalkylsilane (FAS) on its surface. A one-step electrophoretic deposition was applied to fabricate a transparent cross-aligned superhydrophobic TNB/FAS film on a conducting glass substrate. By controlling the deposition time, we have shown the transition between a “sticky” hydrophobic state (high contact angle with strong adhesion) and a “sliding” superhydrophobic state (high contact angle with weak adhesion). The optical transmittance can reach as high as 80% throughout most of the visible light region of the spectrum. These coatings have also displayed high chemical stability and self-cleaning ability. Upon heating the hydrophobic coatings at 500 °C, the TNB coating transforms into a porous TiO<sub>2</sub>(B) structure with superhydrophilic behavior and could be used for anti-fogging applications. With this TiO<sub>2</sub>-based system, we have demonstrated three different wetting states: superhydrophobicity with weak adhesion, high hydrophobicity with strong adhesion, and superhydrophilicity with immediate water spreading. Moreover, this work has also demonstrated superhydrophobic TNB/FAS films with high chemical stability and good self-cleaning performance and superhydrophilic pore-like TiO<sub>2</sub>(B) films with rapid water spreading and excellent anti-fogging ability.

### Introduction

Superhydrophobic surfaces (water contact angle  $\geq 150^\circ$ ) with varying degree of droplet adhesion have attracted great attention from both academic and practical points of view.<sup>1–3</sup> Potential applications such as microfluidics, textiles, self-cleaning and anti-fogging surfaces have been envisaged.<sup>4–11</sup> Superhydrophobic surfaces have been achieved through the control of both chemical composition and morphological structures of the surface.<sup>12–15</sup> To date, many fabrication methods have been proposed to prepare superhydrophobic surfaces, including the sol–gel method, phase separation, layer-by-layer deposition, colloidal self-assembly, and template-based techniques.<sup>16–25</sup> However, many of these fabrication processes involve sophisticated multi-steps and are

often time consuming, which poses a hindrance for practical application. Formation of optically transparent films from organically modified polystyrene spheres or silica particles using the dip-coating method has been reported.<sup>26,27</sup> Nevertheless, so far, it remains a great challenge to generate superhydrophobic surfaces with good transparency and robust stability in both acidic and alkaline media using a simple fabrication process.<sup>26–30</sup>

The electrophoretic deposition (EPD) technique is a well-established industrial process that has been applied for fast deposition of large scale films for applications in medicine, field emitters and so on by using a stable suspension.<sup>31–34</sup> However, the wettability on structured films prepared by EPD has not received much attention so far.<sup>35–37</sup> In the previous work, we had successfully fabricated uniform superhydrophilic titanate nanotube films by combining tetrabutylammonium cation exchange and the EPD process.<sup>35</sup> The resultant highly hydrophobic films with controllable water adhesion were achieved by self-assembly of low-energy materials. Recently, Joung and Buie investigated the wettability of the film by EPD with various suspension stabilities.<sup>36</sup> In their work, a superhydrophobic surface with static contact angle (CA) exceeding 160° and low sliding angle (SA) was constructed with EPD for one minute deposition.

In this work, we present a facile EPD of hydrogen-bond-driven functionalized titanate nanobelts (TNBs) to form stable, transparent and superhydrophobic films in one step. The optimized coating shows not only an excellent superhydrophobicity

<sup>a</sup>School of Materials Science and Engineering, Nanyang Technological University, 50 Nanyang Avenue, Singapore 639798, Singapore. E-mail: aszchen@ntu.edu.sg; Fax: +65 6790 9081; Tel: +65 6790 6727

<sup>b</sup>Physikalisches Institut und Center for Nanotechnology (CeNTech), Westfälische Wilhelms-Universität Münster, Münster D-48149, Germany. E-mail: laiy@uni-muenster.de

<sup>c</sup>State Key Laboratory of Physical Chemistry of Solid Surfaces, and College of Chemistry and Chemical Engineering, Xiamen University, Xiamen 361005, China

† Electronic supplementary information (ESI) available: Video S1 shows the transparent and superhydrophobic TNB/FAS film with extremely low water adhesion; Video S2 shows the self-cleaning ability of the transparent and superhydrophobic TNB/FAS film with extremely low water adhesion. See DOI: 10.1039/c2jm16298a

(CA  $\approx 160^\circ$ ) but also high transparency ( $\sim 76\%$  at 600 nm). Moreover, the coating possesses good chemical stability and self-cleaning performance. By adjusting the coating thickness, adhesion of the highly hydrophobic surface can be tuned from strong adhesion to weak adhesion (e.g. SA  $\leq 10^\circ$ ). After annealing treatment of the TNB film at 500  $^\circ\text{C}$ , the surface changed from superhydrophobic to superhydrophilic when the TNB transforms into a porous  $\text{TiO}_2(\text{B})$  mixed structure. Such a surface has shown rapid water spreading and is potentially useful for anti-fogging applications.

## Experimental section

### Preparation of titanate nanobelt powder

The sodium TNB powders were prepared using a modified hydrothermal method as described in previous reports.<sup>38–40</sup> In a typical synthesis, 0.5 g Degussa P25  $\text{TiO}_2$  powder was uniformly suspended in 75 mL NaOH solution ( $10 \text{ mol L}^{-1}$ ). The solution was then transferred into a 125 mL Teflon-lined autoclave at 200  $^\circ\text{C}$  for 48 h. Subsequently, the as-prepared sodium titanate powder was collected, washed and added to a  $0.1 \text{ mol L}^{-1}$   $\text{HNO}_3$  solution to obtain layered protonated titanate. Finally, the titanate powder was separated by centrifugation and thoroughly washed with distilled water and ethanol five times to completely remove the physically adsorbed ions onto the outer surface of the powder.

### Superhydrophobic hybrid titanate films by electrophoretic deposition

Ethanol solution of  $2.0 \text{ mg mL}^{-1}$  TNB powder and methanolic solution of hydrolyzed 1.0 wt% 1H,1H,2H,2H-perfluorooctyltriethoxysilane ( $\text{CF}_3(\text{CF}_2)_5\text{CH}_2\text{CH}_2\text{Si}(\text{OCH}_2\text{CH}_3)_3$ , FAS, Degussa Co.) with a volume ratio of 4 : 1 were magnetically stirred to obtain a stable opalescent solution by the creation of intermolecular hydrogen interaction between the surface hydroxyl groups and the silanol groups.<sup>41</sup> Prior to the deposition, the substrate, which is an indium tin oxide (ITO) coated glass, was thoroughly cleaned by ultrasonic agitation with acetone, ethanol, and DI water respectively. A  $1.0 \text{ cm}^2$  ITO glass substrate was used as the anode during deposition. A Pt sheet ( $4.0 \text{ cm}^2$ ) was used as the counter (cathode) electrode. The working distance between two electrodes was kept at 2.0 cm.

### Characterization

Scanning electron microscopy (SEM) was performed on a JEOL JSM-7600F field-emission scanning electron microscope. Transmission electron microscopy (TEM) images were collected on a JEOL JEM-2010 transmission electron microscope. X-Ray photoelectron spectroscopy (XPS) was obtained by a VG ESCALAB 250 spectrometer (Thermo Electron, U.K.) to detect the chemical compositions of the coating surface. The binding energies were normalized to the signal for adventitious carbon at 285.0 eV. The X-ray powder diffraction (XRD) analysis was carried out by a Shimadzu 6000 X-ray diffractometer with a Cu K $\alpha$  source. The UV-vis transmittance spectrum was recorded on a UV-1800 spectrophotometer (Shimadzu). The AFM image was obtained by the Dimension 3100 (Veeco, USA) with a Si tip

(resonance frequency: 320 kHz; spring constant:  $42 \text{ N m}^{-1}$ ) in the tapping mode under ambient conditions. Water contact angles (CAs) were measured at ambient temperature using a FTA-1000B contact angle goniometer (First Ten Angstrom, USA), and the values reported were the average of five drops per sample at different locations. The volumes of the droplets used for the static CA and dynamic sliding angle (SA) measurement were 7 and 1  $\mu\text{L}$ , respectively. The pH value of the water solution used for the CA measurement was adjusted using HCl or NaOH.

## Results and discussion

The principle for the preparation of homogeneous and stable TNB/FAS solution is based on the combination of hydrothermal particle formation and hydrogen-bond-driven surface modification of the particle surface, as shown in Fig. 1a. First, water-soluble hydrogen TNBs were obtained *via* a modified hydrothermal treatment of commercially available Degussa P25  $\text{TiO}_2$  nanoparticles. To directly construct a uniform superhydrophobic TNB film by electrophoretic deposition, the TNB particles have to be made hydrophobic and stable in a suspension. However, TNB is hydrophilic in nature, and does not form a stable suspension under the as-synthesized conditions. Therefore, a hydrogen-bond-driven technique was applied to self-assemble low-energy groups of pre-hydrolyzed fluoroalkylsilanol onto the hydroxylated surface of titanate nanobelts to fabricate hydrophobic TNB/FAS powder under magnetic stirring (see ESI, Fig. S1†). A model of the surface chemical group changes during the self-assembly process of FAS on hydroxylated TNB surface as shown in Fig. 2.

Homogeneous hybrid titanate nanobelts were successfully deposited onto the ITO glass to form a uniform TNB/FAS film at 10 V for 2 min (Fig. 1b). FESEM analysis suggests that the as-prepared film is composed of cross-stacked nanobelts parallel to the substrate (Fig. 1c and d). However, the TNB solution without the FAS treatment is not stable in ethanol solution and cannot be successfully electrodeposited under identical conditions. This indicates that the intermolecular interaction between the surface hydroxyl groups ( $-\text{Ti}-\text{OH}$ ) on titanate nanobelts and the fluoroalkylsilanol groups ( $-\text{Si}-\text{OH}$ ) is important for the preparation of stable solution (inset of Fig. 1c) and subsequently the

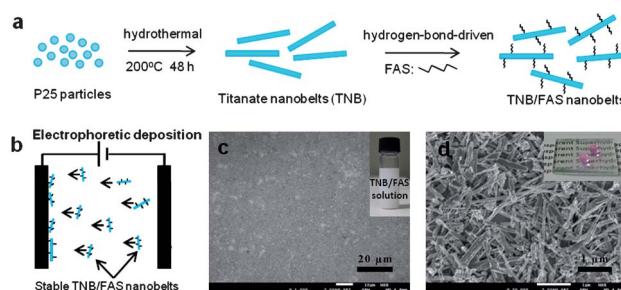


**Fig. 1** (a) Schematic drawing of the synthesis and hydrogen-bond-driven stabilization of titanate nanobelts. (b) Schematic illustration of the electrophoretic deposition process to prepare a TNB/FAS film. (c and d) SEM images of the as-prepared superhydrophobic TNB/FAS film (2 min). The inset images show homogeneous and stable TNB/FAS solution (c) and water droplet on the transparent TNB/FAS film on ITO glass (d).

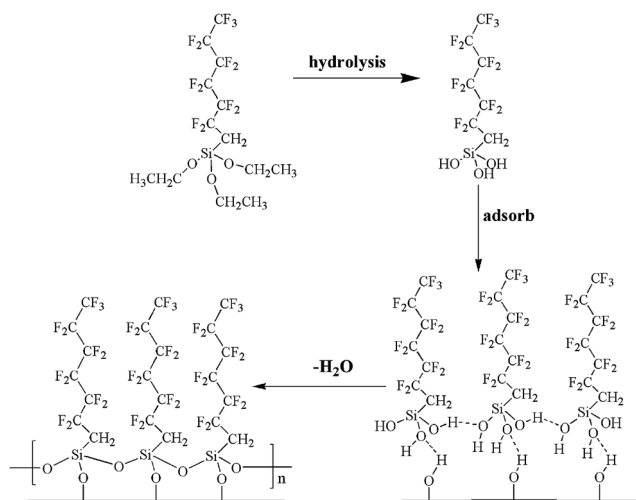


**Fig. 2** Schematic representation of the TNB surface by FAS monolayer grafting to obtain stable TNB/FAS solution.

successful deposition of uniform TNB film with high quality. The water drop formed a perfect spheric shape on the as-prepared transparent TNB/FAS film on ITO substrate. It is noteworthy, comparing the XPS chemical composition before and after the FAS modification (Fig. 3), that the intensities of the F1s and FKLL have increased greatly and those of the Ti2p and O1s decreased to some extent after the FAS modification (Fig. 3a). From the inset high-resolution spectra of C1s and F1s (Fig. 3b), the peaks corresponding to  $-\text{CF}_2$  (at 291.8 eV),  $-\text{CF}_3$  (at 294.1 eV) and a strong fluorine peak (at 690.0 eV) are obviously observed after the FAS modification, suggesting that the fluoroalkyl groups have been assembled onto the titanate nanobelt surfaces.<sup>42</sup>

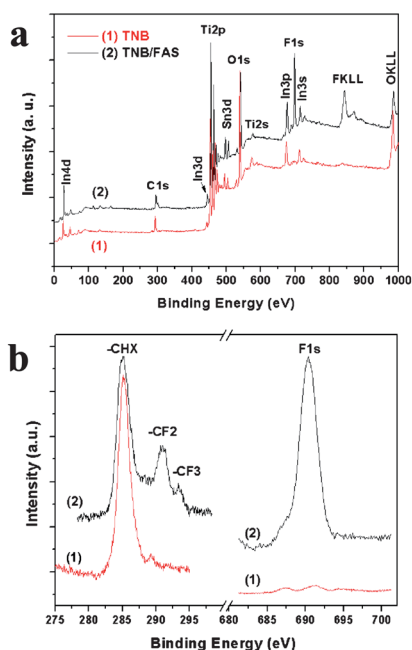


**Fig. 3** Survey (a) and high resolution (b) XPS results of TNB/FAS hybrid film: (1) TNB and (2) TNB/FAS spectra.

FESEM analysis of the effect of deposition time on morphologies indicates that the film structure is consistent with an instantaneous two dimensional (2-D) growth mechanism (Fig. 4). Initially, a layer of sparsely distributed TNB/FAS nanobelts is deposited on the ITO surface (Fig. 4a and d). Subsequently more TNB/FAS nanobelts are deposited onto the surface, forming a layer of continuous compact film (Fig. 4b and e). With longer deposition time, a 3-D densely cross-stacked TNB film with rough surface morphology is formed (Fig. 4c and f). The influence of anodic deposition time on the film morphology is clearly demonstrated through the SEM, AFM (inset of Fig. 4) and profilometric measurements (see ESI, Fig. S2†). There is a general trend of increasing surface roughness with increased deposition time.

The transmittance and wettability of the TNB/FAS hybrid films were evaluated by UV-Vis and water contact angle measurement. As shown in Fig. 5, with the increase in deposition time of TNB/FAS on the conducting glass substrate, a gradual decrease in transmittance was observed. However, the water CA increased greatly to above  $150^\circ$ , which can be attributed to the enhanced roughness and the pores generated by the cross-stacking of TNB particles (see ESI, Fig. S3†). After 1 min deposition, a highly hydrophobic film (CA  $\approx 152.3^\circ$ , see the inset of Fig. 4b) with a roughness about 12.5 nm exhibited a transmittance of  $\sim 76\%$  at a wavelength of 600 nm (Fig. 5b). After 0.5 min deposition, the optical transmittance level was above 80% throughout most of the visible region of the spectrum (Fig. 5a), but the CA dropped to  $141.7^\circ$ . The series of experiments reveals the effect of film coverage and roughness on the transmittance and wettability of the coatings. Based on the results, we could purposely design transparent hydrophobic coatings with the desired level of adhesion as it has been demonstrated that the wettability could be optimized to achieve special high hydrophobicity (CA  $\geq 150^\circ$ ) with ultrahigh or extremely low water SA (Fig. 6).

Fig. 7a–c shows the water droplet image on the strongly adhered hydrophobic TNB/FAS surface (1 min deposition) with different tilting angles. Even when the substrate is vertically aligned or upside down, the water droplet can still firmly adhere to the substrate. The strong adhesion is attributed to the sparse distribution and mostly horizontal alignment of the TNB particles. This has resulted in the direct contact between the water

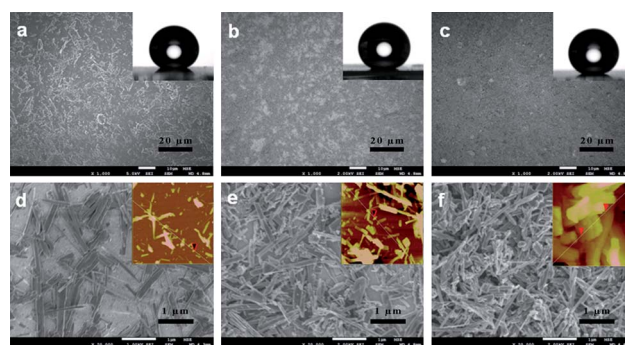


**Fig. 4** SEM images of TNB/FAS hybrid films anodically electrodeposited on ITO substrates at 10 V for 0.5 min (a and d), 1 min (b and e), and 5 min (c and f). Insets in (a)–(c) are the corresponding water drop images. Insets in (d)–(f) are the corresponding AFM images.

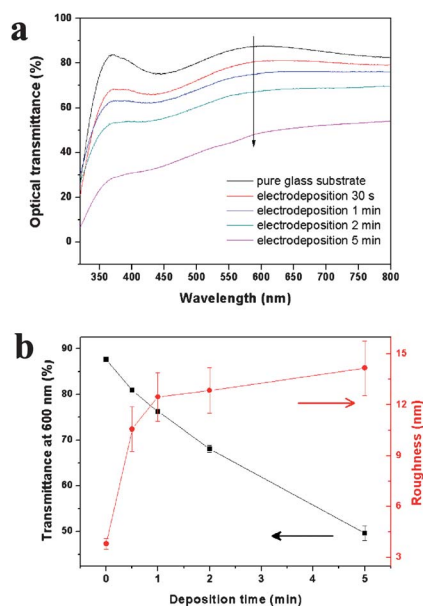


**Fig. 5** (a) The effect of deposition time on transmittance. (b) Transmittance (squares) at 600 nm and roughness (circles) versus deposition time of TNB/FAS hybrid films.

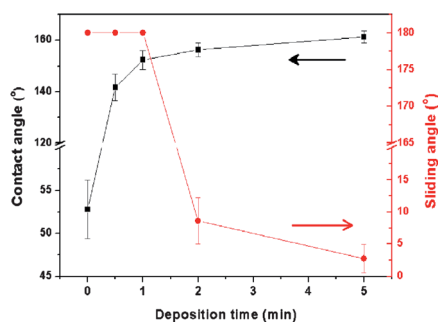


**Fig. 6** The effect of deposition time on the contact angles and sliding angles.

droplet and the partially uncovered hydrophilic substrate, which leads to a typical “sticky” hydrophobic state with a high adhesion (a special case of Wenzel’s state).<sup>43,44</sup> Such a situation is similar to that of the desert beetle whose back has a combination of micro/nanoscale surface roughness and blends with hydrophilic and hydrophobic areas.<sup>45–49</sup> With increased deposition time (2 min), the CA on such a superhydrophobic surface increases to  $\sim 156.2^\circ$  while the dynamic SA drops greatly to approximate  $8.6^\circ$  (Fig. 6). Fig. 7d–f shows another case of superhydrophobic TNB/FAS film by 5 min deposition with low adhesion (see ESI, Video S1†). The water droplets rolled away easily under slight mechanical disturbance (shaking and titling). The dynamic SA of water droplets on such a film with a static CA of  $161.3^\circ$  was lower than  $3^\circ$ . Such a low SA indicates low adhesion between the water droplets and the coating (Cassie’s superhydrophobic state).<sup>44,50</sup>

The CAs of the coatings have not obviously decreased and were maintained at more than  $150^\circ$  even after being soaked in water solution or exposed in ambience for one month. Additionally, the CAs of water droplets with a pH value from 0 to

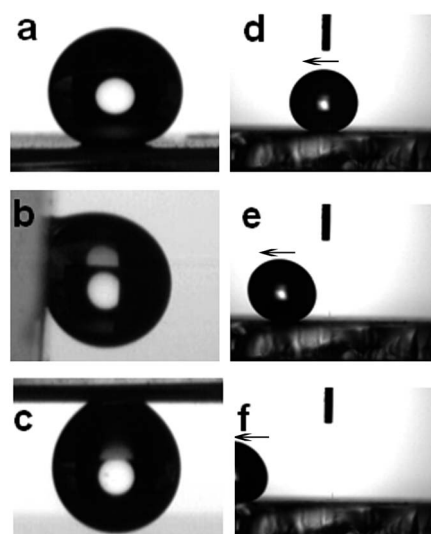


**Fig. 7** Optical images of a water droplet of 7  $\mu\text{L}$  on surfaces of TNB/FAS hybrid films electrodeposited for 1 min with different titling angles: (a)  $0^\circ$ , (b)  $90^\circ$  and (c)  $180^\circ$ . The rolling process (d–f) of a 1  $\mu\text{L}$  water droplet on the surface of TNB/FAS (5 min) which was tilted by  $\sim 3^\circ$  after (d) 0.02 s; (e) 0.04 s; and (f) 0.08 s dropping on to the surface.

14 were measured on the superhydrophobic coating (see Fig. S4 in the ESI†). It shows that the CA remains almost unchanged in such a wide range of pH values from 0 to 14. Such observation indicates that the superhydrophobic TNB/FAS coating had good chemical stability. This is because of the chemically inert nature of the FAS coating which has strong  $-\text{CF}_3$  terminal groups. The air trapped in the pores of the surface layer further reduces the direct contact between the liquid and solid, rendering TNB/FAS coatings with good stability.<sup>50,51</sup> An exception to the stable TNB/FAS films occurred in the basic solution of pH 14 for an extended soaking time of about ten minutes, which is due to the cleavage of the Si–O bonds in the FAS monolayer by the strong alkaline solution and the resultant exposure of the uncovered substrate.<sup>41</sup>

The self-cleaning performance of the transparent and highly superhydrophobic surface (Fig. 8a and Video S2†) was demonstrated with yellow nitrogen-doped titanate powder as a model dust/contaminant. The self-cleaning process is shown in Fig. 8b. A sparse layer of contaminant powder was sprinkled on the surface and then a water droplet was placed on the contaminated surface. During the sliding process (Fig. 8b), the contaminant powder was immediately picked up and carried away by the water droplet, leaving behind a clear surface. It was observed that the water droplet maintained a spherical shape even after it has taken up the contaminant. This observation confirms that the high water surface tension and low surface energy of TNB/FAS coating played an important role in adsorbing contaminants, and one small water droplet could clean up a large amount of contaminants until its surface is fully saturated.

Lastly, we demonstrate how to convert the as-deposited superhydrophobic TNB/FAS coatings to superhydrophilic ones. Taking a 2 min coated TNB/FAS sample as an example; after a short thermal treatment at  $500^\circ\text{C}$ , the water droplet completely spread and permeated into the coating within 0.24 s, suggesting

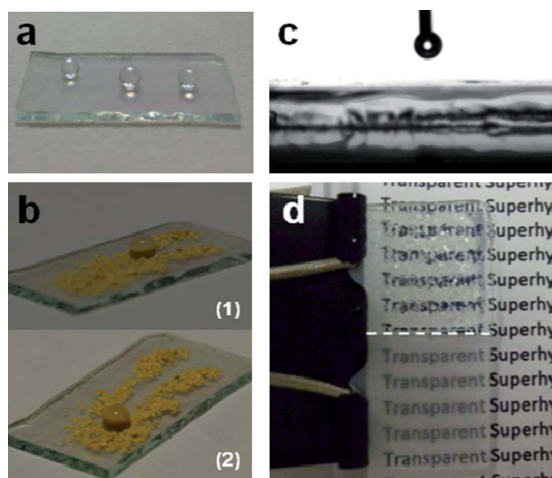


**Fig. 8** (a) Image of water droplets slightly dropped on a conducting substrate covered with a TNB film deposited for 5 min. (b) Time sequence of the self-cleaning process on the superhydrophobic coating with low water adhesion. (c) Water droplet on the superhydrophilic  $\text{TiO}_2(\text{B})$  film. (d) Photograph of an ITO substrate deposited with superhydrophilic coatings (bottom) and a control ITO substrate without any coating deposition (upper) taken from a refrigerator ( $-4\text{ }^\circ\text{C}$ ) to the humid laboratory air (ca. 50% RH).

that the coating has become superhydrophilic (Fig. 8c). After the heat treatment, the FAS monolayer has been completely decomposed, and at the same time, the TNB was found to have transformed into the  $\text{TiO}_2(\text{B})$  crystal structure while maintaining the nanobelts morphology with nanopores. The pores were obviously formed due to the loss of water in hydrogen titanate.<sup>52–54</sup> Previous studies predicted and verified that superhydrophilic coatings can be obtained by increasing the surface roughness of a hydrophilic coating.<sup>12–15</sup> We believe that the addition of the nanopores to the micro-stacked morphology is a key factor for the transition to superhydrophilic in the current work too. The HRTEM images (Fig. 9) confirm that the morphology of the dense titanate nanobelts has changed to the porous  $\text{TiO}_2(\text{B})$  and anatase  $\text{TiO}_2$  nanobelts after the heat treatment. The lattice spacing distance between the planes parallel to the longitudinal nanobelt direction is measured to be 0.78 nm, which agrees with the (200) *d*-space of layered hydrogen titanate. After annealing, a smaller (001) interplanar spacing (0.63 nm) is in good agreement with the *d*-space of the (001)  $\text{TiO}_2(\text{B})$  planes. Fig. 10 shows XRD patterns of the titanate powders before and after the 500 °C annealing. Peaks marked “H”, “B” and “A” correspond to hydrogen titanate,  $\text{TiO}_2(\text{B})$  and anatase  $\text{TiO}_2$  phase respectively. The main structure of the as-prepared hydrogen titanate is similar to that of a layered trititanate ( $\text{H}_2\text{Ti}_3\text{O}_7$ , JCPDS 41-0192). Many narrow diffraction peaks indexed to  $\text{TiO}_2(\text{B})$  (JCPDS 46-1237) and some other diffraction peaks indexed to anatase  $\text{TiO}_2$  (JCPDS 21-1272) can be clearly identified. The cross-stacked nanobelts and the high porosity inside the  $\text{TiO}_2(\text{B})$  nanobelts greatly increase the actual surface area and thus the surface roughness of the coating. The rough and porous cross-stacking structures provide plentiful capillary percolation channels to water permeation through the hydrophilic  $\text{TiO}_2(\text{B})$  coatings, resulting in the superhydrophilic performance of the film with rapid

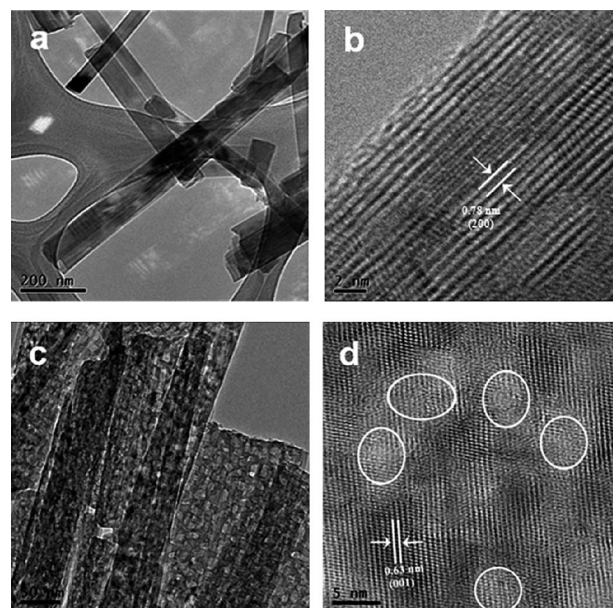


**Fig. 9** TEM images of the titanate nanobelts before (a and b) and after annealing (c and d). The mesopores in (d) were noted by white circles.

water spreading in several hundreds of milliseconds (see ESI, Fig. S5†). Moreover, the superhydrophilic  $\text{TiO}_2(\text{B})$  film becomes superhydrophobic by the same FAS modification used for TNB. This indicates that the  $\text{TiO}_2(\text{B})$  films can be reversibly controlled from superhydrophobicity to superhydrophilicity by the simple FAS modification and thermal treatment, respectively. The antifogging performance of the cross-stacked superhydrophilic  $\text{TiO}_2(\text{B})$ /anatase composite coatings was demonstrated by exposing it to humid laboratory air (ca. 50% RH) after storage at  $-4\text{ }^\circ\text{C}$  in a refrigerator. As shown in Fig. 8d, the bare quartz slide (upper) fogged immediately and the words below are blurred by strong light scattering. In contrast, the slide coated with the  $\text{TiO}_2(\text{B})$  composite films (bottom) can significantly prevent fogging formation by almost instantaneously spreading the condensed water droplets to form a thin water membrane. Therefore, the slide with the  $\text{TiO}_2(\text{B})$  coated glass remains highly transparent and the words below are clearly seen.

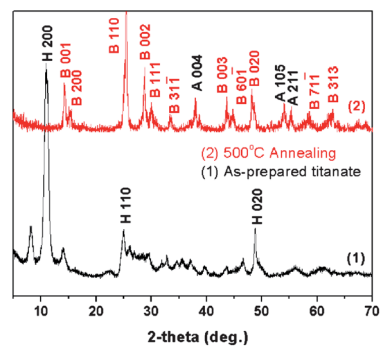


**Fig. 10** XRD of the TNB/FAS hybrid powder before and after 500 °C annealing. H stands for hydrogen titanate, B for  $\text{TiO}_2(\text{B})$  and A for anatase  $\text{TiO}_2$ .

## Conclusions

In summary, we report an electrophoretic deposition method to form homogeneous and stable TiO<sub>2</sub>-based nanobelt thin films. The cross-stacked TNB films, self-assembled with a monolayer of FAS organic molecules, have demonstrated superhydrophobicity, good transparency, and excellent chemical stability in a wide range of pH solutions. By adjusting the deposition time, the superhydrophobic coatings can be made “sticky” and “non-sticky” for the water droplet on the surface, from which various potential applications can be derived (e.g. self-cleaning). Upon heat treatment, the superhydrophobic surface can be turned into superhydrophilic, with the transformation of the hydrogen titanate to porous TiO<sub>2</sub>(B) and anatase TiO<sub>2</sub>. Therefore in this TiO<sub>2</sub>-based material system, we have demonstrated realization of three very different wetting states, viz. highly hydrophobic with strong adhesion, superhydrophobic with weak adhesion, and superhydrophilic with rapid water spreading. We can envisage their application to a wide range of applications such as micro-droplet transportation, self-cleaning, anti-fogging, ultra-fast spreading for biomolecules analysis, ultra-fast absorption in printing and so on.

## Acknowledgements

The authors thank the Environment and Water Industry Programme Office (EWI) under the National Research Foundation of Singapore (grant MEWR651/06/160), the National Nature Science Foundation of China (20773100, 51072170 and 20620130427), and National Basic Research Program of China (973 Program) (2007CB935603) for the financial support of the work, and the Alexander von Humboldt (AvH) Foundation of Germany (Y. Lai) for the financial support of the work.

## References

- 1 M. J. Liu, Y. M. Zheng, J. Zhai and L. Jiang, *Acc. Chem. Res.*, 2010, **43**, 368–377.
- 2 M. J. Liu and L. Jiang, *Adv. Funct. Mater.*, 2010, **20**, 3753–3764.
- 3 Y. K. Lai, X. F. Gao, H. F. Zhuang, J. Y. Huang, C. J. Lin and L. Jiang, *Adv. Mater.*, 2009, **21**, 3799–3803.
- 4 X. Zhang, F. Shi, J. Niu, Y. G. Jiang and Z. Q. Wang, *J. Mater. Chem.*, 2008, **18**, 621–633; F. Shi, Z. Q. Wang and X. Zhang, *Adv. Mater.*, 2005, **17**, 1005–1009.
- 5 X. Yao, Y. L. Song and L. Jiang, *Adv. Mater.*, 2011, **23**, 719–734; Q. W. Chen, X. Yao, L. Xu, Q. K. Li, Y. L. Song and L. Jiang, *Soft Matter*, 2010, **6**, 2470–2474.
- 6 D. Wu, S. Z. Wu, Q. D. Chen, Y. L. Zhang, J. Yao, X. Yao, L. G. Niu, J. N. Wang, L. Jiang and H. B. Sun, *Adv. Mater.*, 2011, **23**, 545–549.
- 7 X. J. Liu, M. R. Cai, Y. M. Liang, F. Zhou and W. M. Liu, *Soft Matter*, 2011, **7**, 3331–3336; X. J. Liu, Q. A. Ye, X. W. Song, Y. W. Zhu, X. L. Cao, Y. M. Liang and F. Zhou, *Soft Matter*, 2011, **7**, 515–523.
- 8 G. McHale and M. I. Newton, *Soft Matter*, 2011, **7**, 5473–5481.
- 9 M. Wang, C. Chen, J. P. Ma and J. Xu, *J. Mater. Chem.*, 2011, **21**, 6962–6967.
- 10 X. D. Zhao, H. M. Fan, X. Y. Liu, H. H. Pan and H. Y. Xu, *Langmuir*, 2011, **27**, 3224–3228.
- 11 J. Li, X. H. Liu, Y. P. Ye, H. D. Zhou and J. M. Chen, *J. Phys. Chem. C*, 2011, **115**, 4726–4729.
- 12 L. Feng, S. H. Li, Y. S. Li, H. J. Li, L. J. Zhang, J. Zhai, Y. L. Song, B. Q. Liu, L. Jiang and D. B. Zhu, *Adv. Mater.*, 2002, **14**, 1857–1860; T. L. Sun, L. Feng, X. F. Gao and L. Jiang, *Acc. Chem. Res.*, 2005, **38**, 644–652.
- 13 A. Lafuma and D. Quéré, *Nat. Mater.*, 2003, **2**, 457–460.
- 14 M. L. Ma and R. M. Hill, *Curr. Opin. Colloid Interface Sci.*, 2006, **11**, 193–202.
- 15 M. Nosonovsky and B. Bhushan, *Curr. Opin. Colloid Interface Sci.*, 2009, **14**, 270–280; M. Nosonovsky and B. Bhushan, *Adv. Funct. Mater.*, 2008, **18**, 843–855.
- 16 H. Y. Erbil, A. L. Demirel, Y. Avci and O. Mert, *Science*, 2003, **299**, 1377–1380.
- 17 X. M. Li, D. Reinhoudt and M. Crogo-Calama, *Chem. Soc. Rev.*, 2007, **36**, 1350–1368.
- 18 P. Roach, N. J. Shirtcliffe and M. I. Newton, *Soft Matter*, 2008, **4**, 224–240.
- 19 K. S. Liu, X. Yao and L. Jiang, *Chem. Soc. Rev.*, 2010, **39**, 3240–3255.
- 20 Z. G. Guo, W. M. Liu and B. L. Su, *J. Colloid Interface Sci.*, 2011, **353**, 335–355.
- 21 M. J. Xu, N. Lu, H. B. Xu, D. P. Qi, Y. D. Wang, S. L. Shi and L. F. Chi, *Soft Matter*, 2010, **6**, 1438–1443.
- 22 J. Yang, Z. Z. Zhang, X. H. Men, X. H. Xu and X. T. Zhu, *J. Colloid Interface Sci.*, 2010, **346**, 241–247.
- 23 W. Lee, B. G. Park, D. H. Kim, D. J. Ahn, Y. Park, S. H. Lee and K. B. Lee, *Langmuir*, 2010, **26**, 1412–1415.
- 24 X. H. Chen, L. H. Kong, D. Dong, G. B. Yang, L. G. Yu, J. M. Chen and P. Y. Zhang, *J. Phys. Chem. C*, 2009, **113**, 5396–5401.
- 25 P. Wang, R. Qiu, D. Zhang, Z. F. Lin and B. R. Hou, *Electrochim. Acta*, 2010, **56**, 517–522.
- 26 A. Nakajima, K. Hashimoto, T. Watanabe, K. Takai, G. Yamauchi and A. Fujishima, *Langmuir*, 2000, **16**, 7044–7047; A. Nakajima, A. Fujishima, K. Hashimoto and T. Watanabe, *Adv. Mater.*, 1999, **11**, 1365–1368.
- 27 Q. F. Xu, J. N. Wang and K. D. Sanderson, *ACS Nano*, 2010, **4**, 2201–2209; Q. F. Xu, J. N. Wang, I. H. Smith and K. D. Sanderson, *J. Mater. Chem.*, 2009, **19**, 655–660.
- 28 J. A. Howarter and J. P. Youngblood, *Macromol. Rapid Commun.*, 2008, **29**, 455–466; A. V. Rao, S. S. Latthe, D. Y. Nadargi, H. Hirashima and V. Ganesan, *J. Colloid Interface Sci.*, 2009, **332**, 484–490; Y. H. Xiu, F. Xiao, D. W. Hess and C. P. Wong, *Thin Solid Films*, 2009, **517**, 1610–1615.
- 29 H. Yabu and M. Shimomura, *Chem. Mater.*, 2005, **17**, 5231–5234.
- 30 A. Tricoli, M. Righettoni and S. E. Pratsinis, *Langmuir*, 2009, **25**, 12578–12584; X. Y. Ling, I. Y. Phang, G. J. Vancso, J. N. Huskens and D. N. Reinhoudt, *Langmuir*, 2009, **25**, 3260–3263.
- 31 B. Gao, G. Z. Yue, Q. Qiu, Y. Cheng, H. Shimoda, L. Fleming and O. Zhou, *Adv. Mater.*, 2001, **13**, 1770–1773.
- 32 P. Sarkar and P. S. Nicholson, *J. Am. Chem. Soc.*, 1996, **79**, 1987–2002.
- 33 I. Zhitomirsky and L. GalOr, *J. Mater. Sci.: Mater. Med.*, 1997, **8**, 213–219.
- 34 M. Hologado, F. Garcia-Santamaria, A. Blanco, M. Ibisate, A. Cintas, H. Miguez, C. J. Serna, C. Molpeceres, J. Requena, A. Mifsud, F. Meseguer and C. Lopez, *Langmuir*, 1999, **15**, 4701–4704.
- 35 Y. K. Lai, Y. C. Chen, Y. X. Tang, D. G. Gong, Z. Chen and C. J. Lin, *Electrochem. Commun.*, 2009, **11**, 2268–2271.
- 36 Y. S. Joung and C. R. Buie, *Langmuir*, 2011, **27**, 4156–4163.
- 37 H. Ogihara, J. Okagaki and T. Saji, *Chem. Lett.*, 2009, **38**, 132–133.
- 38 T. Kasuga, M. Hiramatsu, A. Hoson, T. Sekino and K. Niihara, *Langmuir*, 1998, **14**, 3160–3163.
- 39 D. J. Yang, H. W. Liu, Z. F. Zheng, Y. Yuan, J. C. Zhao, E. R. Waclawik, X. B. Ke and H. Y. Zhu, *J. Am. Chem. Soc.*, 2009, **49**, 17885–17893.
- 40 Y. X. Tang, D. G. Gong, Y. K. Lai, Y. Q. Shen, Y. Y. Zhang, Y. Z. Huang, J. Tao, C. J. Lin, Z. L. Dong and Z. Chen, *J. Mater. Chem.*, 2010, **20**, 10169–10178.
- 41 Y. K. Lai, Y. X. Tang, J. Y. Huang, H. Wang, H. Q. Li, D. G. Gong, X. B. Ji, J. J. Gong, C. J. Lin, L. Sun and Z. Chen, *Soft Matter*, 2011, **7**, 6313–6319.
- 42 Y. K. Lai, C. J. Lin, H. Wang, J. Y. Huang, H. F. Zhuang and L. Sun, *Electrochem. Commun.*, 2008, **10**, 387–391.
- 43 R. N. Wenzel, *Ind. Eng. Chem.*, 1936, **28**, 988–994.
- 44 S. T. Wang and L. Jiang, *Adv. Mater.*, 2007, **19**, 3423–3424.
- 45 A. R. Parker and C. R. Lawrence, *Nature*, 2001, **414**, 33–34.
- 46 L. Zhai, M. C. Berg, F. C. Cebeci, Y. Kim, J. M. Milwid, M. F. Rubner and R. E. Cohen, *Nano Lett.*, 2006, **6**, 1213–1217.
- 47 D. A. Wang, Y. Liu, X. J. Liu, F. Zhou, W. M. Liu and Q. J. Xue, *Chem. Commun.*, 2009, (45), 7018–7020.
- 48 Y. K. Lai, Z. Q. Lin, J. Y. Huang, L. Sun, Z. Chen and C. J. Lin, *New J. Chem.*, 2010, **34**, 44–51; Y. K. Lai, Y. X. Huang, H. Wang,

- 
- J. Y. Huang, Z. Chen and C. J. Lin, *Colloids Surf., B*, 2010, **76**, 117–122.
- 49 B. Balu, V. Breedveld and D. W. Hess, *Langmuir*, 2008, **24**, 4785–4790.
- 50 A. B. D. Cassie and S. Baxter, *Trans. Faraday Soc.*, 1944, **40**, 546–551.
- 51 Y. K. Lai, C. J. Lin, J. Y. Huang, H. F. Zhuang, L. Sun and T. Nguyen, *Langmuir*, 2008, **24**, 3867–3873.
- 52 Q. J. Li, J. W. Zhang, B. B. Liu, M. Li, R. Liu, X. L. Li, H. L. Ma, S. D. Yu, L. Wang, Y. G. Zou, Z. P. Li, T. Cui and G. T. Zou, *Inorg. Chem.*, 2008, **47**, 9870–9873.
- 53 Z. F. Zheng, H. W. Liu, J. P. Ye, J. C. Zhao, E. R. Waclawik and H. Y. Zhu, *J. Mol. Catal. A: Chem.*, 2010, **316**, 75–82.
- 54 W. Q. Han, L. J. Wu, R. F. Klie and Y. M. Zhu, *Adv. Mater.*, 2007, **19**, 2525–2529.